Numerical Investigation of Strongly Interacting Bosons at Zero Temperature

Laurent de Forges de Parny   Frank Schäfer   Jonas Mielke

Miguel A. Bastarrachea-Magnani   Andreas Buchleitner

Physikalisches Institut, Albert-Ludwigs-Universität Freiburg, Germany

We review some numerical works carried out within the department for Quantum Optics and Statistics at the University of Freiburg's Institute of Physics, between September 2016 and June 2018. Our activities focus on quantum properties of matter at zero temperature, i. e., a regime where the thermal energy $k_B T$ is negligible with respect to the other energy scales of the considered system. This area of research, related to ultracold gases, has attracted a great deal of interest, both experimentally and theoretically, since the first realization of a Bose-Einstein condensate in 1995. In a context where the theoretical understanding of these systems still remains challenging, the growing power of computers offers a unique and efficient way to tackle such challenges. In our theory group, we particularly use powerful numerical methods that give *exact* results, in contrast to other theoretical approaches based on an *a priori* assumption, e. g., mean-field theory. To illustrate it, we focus on few typical results that would not be available other than by using high-performance computing. These results have been obtained by using three numerical methods: quantum Monte Carlo (QMC), Gutzwiller Monte Carlo (GMC), and the Multiconfigurational Time-dependent Hartree method for bosons (MCTDHX).

1 Introduction

In the last century, high-performance computing has been of crucial importance in theoretical and applied sciences, e.g., for meteorological predictions and for nuclear studies. More precisely, the Manhattan project during World War II, is considered the starting point in the field of numerical computation. Then, the civil Fermi-Pasta-Ulam numerical simulation in 1953 definitely opened the perspective of solving physical problems not solvable otherwise (Dauxois et al., 2005). Nowadays, numerical simulations are used extensively in many fields of Science: Monte Carlo methods in statistical physics, particle physics, quantum chemistry, econometrics, *etc.*; Finite elements and Runge-Kutta for solving differential equations in mathematics, physics and for star and galaxy dynamics in astrophysics; Particle-in-Cell simulations and molecular dynamics in Biology, *etc.* (Ferrario et al., 2006).

In low-energy physics, numerical simulations are very practical tools for solving Hamiltonian models under active investigation in condensed matter and ultracold gases. The main constraint remains the diagonalization of the Hamiltonian matrix, a mathematical operation circumvented by many technics, e.g. exact diagonalization if possible, auxiliary-field, variational and quantum Monte Carlo, dynamical mean-field theory, the density matrix renormalization group (DMRG), and, more recently, tensor networks, MCTDHX and the time-DMRG (Dagotto, 1994; Scalapino, 2006; Román, 2014).

In this paper, we discuss a panel of numerical methods we used within the department for Quantum Optics and Statistics at the University of Freiburg's Institute of Physics, between September 2016 and June 2018. These methods allowed for extensive simulations of interacting bosons in a regime where the thermal energy $k_B T$ is negligible with respect to the energy scale of the Hamiltonian terms, i.e., in the zero temperature limit. The paper is organized as follows: In Sec. 2, we discuss the QMC method and the stochastic Green functions in the context of quantum magnetism. In Sec. 3, we present the GMC method: a flexible – but non-exact – numerical method we have developed and used for studying a recent system of interacting bosons placed in an optical lattice and inside a high-finesse optical cavity. Sec. 4 reports our dynamical investigation of ultracold bosons in a time-dependent double-well potential with the MCTDHX method. In Sec. 5, we summarize these results and give some final remarks.

2 QMC method: application to Bose-Einstein condensate with magnetic interactions

High-temperature superconductivity remains a central problem in solid-state physics. Although actively under investigation since the 90s, this phenomenon, which involves electricity transport without losing energy, is not described by a unique theory. The mechanism of superconductivity is inherent to quantum mechanics: free electrons – which are fermionic particles – are bound in pairs, called Cooper pairs, due to their interactions with the ionic lattice. The resulting Cooper pairs behave like bosons and condense into the ground state to form a Bose-Einstein condensate.[1] The consideration of the particles interactions are essential for the understanding of this mechanism. In this context, the Hubbard model, originally developed in 1963 to describe electrons in solids, has been proposed as a promising candidate for the understanding of high-temperature superconductivity (Nature Physics, 2013). Nevertheless, an exact solution exists only in 1D and higher-dimensional materials, i. e. most of the existing materials, are difficult to investigate. Once paired, the Cooper pairs lead to interacting bosons in an ionic lattice well described by the Bose-Hubbard model. This particularly simple model has not ceased to intrigue theoretical condensed-matter physicists, as the physics described by this model is rich and surprising. Indeed, it captures the essence of the paradigmatic superfluid-insulator transition, a transition of high interest in solid-state physics (Fisher et al., 1989). Since a general analytical solution of the (Bose)-Hubbard model does not exist in 2D and 3D, many computational techniques have been developed, e. g. quantum Monte Carlo, dynamical mean-field theory, and tensor networks, to cite a few (Dagotto, 1994; Scalapino, 2006; Román, 2014).

A remarkable idea in the context of atomic physics was the proposal in 1998 to implement the Bose-Hubbard model by loading a Bose-Einstein condensate into an optical lattice (Jaksch et al., 1998). This seminal idea has opened new perspectives in the field of quantum phase transition and led to the first observation of the Mott-superfluid transition in 2002 (Greiner et al., 2002). Subsequently, these experiments made possible the achievement of low-dimensional systems where new phases can emerge (Bloch et al., 2008). In particular, these systems allow for the investigation of more complex models, called *extended* Bose-Hubbard models, which

---

[1]cf. BCS theory, Nobel Prize in Physics in 1972.

consider additional ingredients like spin-spin interactions. This opens the possibility to investigate the interplay between magnetism and superfluidity (Vengalattore, Leslie et al., 2008; Vengalattore, Guzman et al., 2010) and, more recently, quantum phase transitions with spin degrees of freedom (Jiang et al., 2016).

We focus here on a spin-1 bosonic model for which a quantum magnetic state, the nematic state, arises from the magnetic interactions. This non-trivial nematic state is particularly surprising since the spin-rotation symmetry is spontaneously broken without magnetic ordering: the spins are randomly anti-aligned and the total magnetization vanishes (Zibold et al., 2016; Jacob et al., 2012; Forges de Parny, Yang et al., 2014). The extended Bose-Hubbard Hamiltonian describing this model reads (Mahmud et al., 2013; Imambekov et al., 2003; Imambekov et al., 2004; Ho, 1998)

$$
\hat{\mathcal{H}} = -t \underbrace{\sum_{\sigma,\langle \mathbf{r},\mathbf{r}'\rangle} \left(a_{\sigma\mathbf{r}}^{\dagger} a_{\sigma\mathbf{r}'} + \text{h.c.} \right)}_{\text{kinetic term}} + \underbrace{\frac{U_0}{2} \sum_{\mathbf{r}} \hat{n}_{\mathbf{r}} \left(\hat{n}_{\mathbf{r}} - 1 \right)}_{\text{on-site repulsion}} + \underbrace{\frac{U_2}{2} \sum_{\mathbf{r}} \left(\hat{\mathbf{S}}_{\mathbf{r}}^2 - 2\hat{n}_{\mathbf{r}} \right)}_{\text{on-site spin-spin interaction}}
$$
$$
- \underbrace{q \sum_{\mathbf{r}} \hat{n}_{0\mathbf{r}}}_{\text{quadratic Zeeman}} - \underbrace{\mu \sum_{\sigma,\mathbf{r}} \hat{n}_{\sigma\mathbf{r}}}_{\text{chemical potential}} \quad , \tag{1}
$$

where operator $a_{\sigma\mathbf{r}}$ ($a_{\sigma\mathbf{r}}^{\dagger}$) annihilates (creates) a boson in the Zeeman state $\sigma = \{\pm 1, 0\}$ on site $\mathbf{r}$ of a periodic square optical lattice of size $L \times L$. The kinetic term allows particles to hop between neighboring sites $\langle \mathbf{r}, r' \rangle$ with strength t. $N_{\sigma} \equiv \sum_{\mathbf{r}} \langle a_{\sigma\mathbf{r}}^{\dagger} a_{\sigma\mathbf{r}} \rangle$ denotes the total number of σ bosons, $\rho_{\sigma} \equiv N_{\sigma}/L^2$ the corresponding density, and $\rho \equiv \sum_{\sigma} \rho_{\sigma}$ the total density. The operator $\hat{\mathbf{S}}_{\mathbf{r}} = (\hat{S}_{x,\mathbf{r}}, \hat{S}_{y,\mathbf{r}}, \hat{S}_{z,\mathbf{r}})$ is the spin operator where $\hat{S}_{\alpha,\mathbf{r}} = \sum_{\sigma,\sigma'} a_{\sigma\mathbf{r}}^{\dagger} J_{\alpha,\sigma\sigma'} a_{\sigma'\mathbf{r}}$, $\alpha = \{x, y, z\}$ and the $J_{\alpha,\sigma\sigma'}$ are standard spin-1 matrices. The parameters $U_0 > 0$ and U_2 are the on-site spin-independent and spin-dependent interaction terms. In the following, we will consider antiferromagnetic $^{23}\text{N}a$ atoms for which $U_2/U_0 \simeq 0.036$. For these atoms, the local magnetic moment $S^2(0) \equiv \frac{1}{L^2} \sum_{\mathbf{r}} \langle \hat{\mathbf{S}}_{\mathbf{r}}^2 \rangle$ is minimized, which means that the spins of atoms anti-align to form a singlet if possible. Finally, μ is the chemical potential. We have previously derived the exact phase diagram without considering the quadratic Zeeman term, i.e., for $q = 0$, and investigate the properties of the nematic state (Forges de Parny, Yang et al., 2014; Forges de Parny, Hébert et al., 2013). The purpose of our recent study was to show that the quadratic Zeeman effect – a control parameter in experiments – is a

control parameter for tuning the nematic state and the Mott-superfluid transition (Forges de Parny and Rousseau, 2018). In the following, we discuss our numerical approach to tackling this question.

According to standard quantum mechanic rules, all the physical information is obtained by diagonalizing the Hamiltonian matrix associated with operator Eq. (1). Typically, in a bi-dimensional lattice experiment, $N \sim 10^5$ atoms are trapped in $\sim 10^8$ sites. The square matrix to diagonalize has a size of $\sim 10^{300000} \times 10^{300000}$ which is far from the total estimated number of atoms in our known Universe, i.e., 10^{80} atoms. Even if the Hamiltonian matrix is sparse, its diagonalization is impossible. To overcome this problem, we have used a powerful numerical method, the quantum Monte Carlo method, which gives exact results for the most probable state at equilibrium, i.e., the ground state $|\psi_g\rangle$ (Forges de Parny, Hébert et al., 2013; Forges de Parny and Rousseau, 2018). Like all methods, this one has its own limitations: the sign problem (Loh et al., 1990), long time convergence and CPU time cost, implementation difficulties, etc. Nevertheless, using the NEMO cluster and parallelized simulations, we were able to investigate $N = 288$ interacting bosons in $L \times L = 144$ sites, i.e., a system described by a Hamiltonian matrix of size $\sim 10^{118} \times 10^{118}$ which is far beyond the limits of the exact diagonalization methods (even with the Lanczos algorithm). More technically, for $N = 288$ bosons in $L \times L = 144$ sites, we obtained converged results with a thermalization time of 10 hours and a measurement time of 1 day and 10 hours, using MPI parallelized simulations with 20 processors per node and $2\,\mathrm{GB}$ of persistent memory on bwForCluster NEMO. Typically, the total ground state energy $E_g = \langle\psi_g|\hat{\mathcal{H}}|\psi_g\rangle$ – which converges faster than other quantities – is converged with an accuracy of 0.001%.

We have used QMC simulations with the stochastic Green function (SGF) algorithm, developed by Valy Rousseau (Rousseau, 2008). Whereas most of the QMC algorithms sample the partition function $\mathcal{Z}(\beta) = \sum_\psi \langle\psi|e^{-\beta\hat{\mathcal{H}}}|\psi\rangle$ (Fehske et al., 2007; Sandvik, 2010), with $\beta = 1/k_B T$ the inverse of temperature, the SGF algorithm samples the *extended* partition function

$$\mathcal{Z}(\beta,\tau) = \sum_\psi \langle\psi|e^{-(\beta-\tau)\hat{\mathcal{H}}}\hat{\mathcal{G}}e^{-\tau\hat{\mathcal{H}}}|\psi\rangle \; , \tag{2}$$

where $\hat{\mathcal{G}}$ is the the Green operator defined by

$$\hat{\mathcal{G}} = \sum_{p=0}^{+\infty}\sum_{q=0}^{+\infty} g_{pq} \sum_{\{i_p|j_q\}} \prod_{k=1}^{p} \hat{\mathcal{A}}_{i_k}^{\dagger} \prod_{l=1}^{q} \hat{\mathcal{A}}_{j_l}. \tag{3}$$

In Eq. (3), the notation $\{i_p|j_q\}$ denotes two subsets of site indices $i_1, i_2, \cdots, i_p$ and $j_1, j_2, \cdots, j_q$ with the constraint that all indices in subset i are different from the indices in subset j (but several indices in one subset may be equal), and g_{pq} is a matrix that depends on the application of the algorithm. In the occupation number representation, the normalized creation and annihilation operators,

$$\hat{\mathcal{A}}^{\dagger} = a^{\dagger}\frac{1}{\sqrt{\hat{n}+1}} \qquad \hat{\mathcal{A}} = \frac{1}{\sqrt{\hat{n}+1}}a, \tag{4}$$

satisfy the following relations for any state $|n\rangle$,

$$\hat{\mathcal{A}}^{\dagger}|n\rangle = |n+1\rangle \qquad \hat{\mathcal{A}}|n\rangle = |n-1\rangle, \tag{5}$$

with the particular case $\hat{\mathcal{A}}|0\rangle = 0$. The SGF algorithm can be applied to any lattice Hamiltonian of the form $\hat{\mathcal{H}} = \hat{\mathcal{V}} - \hat{\mathcal{T}}$, where $\hat{\mathcal{V}}$ is diagonal in the chosen occupation number basis and $\hat{\mathcal{T}}$ has only positive matrix elements (to avoid the sign problem). The extended partition function, expressed in terms of Feynman path integrals in continuous imaginary time, takes the form

$$\begin{aligned} \mathcal{Z}(\beta,\tau) &= \sum_{n\geq 0}\int_{0<\tau_1<\cdots<\tau_n<\beta} \langle\psi_0|e^{-\beta\mathcal{V}}\hat{\mathcal{T}}(\tau_n)|\psi_{n-1}\rangle\langle\psi_{n-1}|\hat{\mathcal{T}}(\tau_{n-1})|\psi_{n-2}\rangle \\ &\times\cdots\langle\psi_{L+1}|\hat{\mathcal{T}}(\tau_L)|\psi_L\rangle\langle\psi_L|\hat{\mathcal{G}}(\tau)|\psi_R\rangle\langle\psi_R|\hat{\mathcal{T}}(\tau_R)|\psi_{R-1}\rangle \\ &\times\cdots\langle\psi_2|\hat{\mathcal{T}}(\tau_2)|\psi_1\rangle\langle\psi_1|\hat{\mathcal{T}}(\tau_1)|\psi_0\rangle d\tau_1\cdots d\tau_n, \end{aligned} \tag{6}$$

where the sum $\sum_{n\geq 0}$ implicitly runs over complete sets of states $\{|\psi_k\rangle\}$, and $\hat{\mathcal{T}}(\tau)$ and $\hat{\mathcal{G}}(\tau)$ the time-dependent operators defined by

$$\hat{\mathcal{T}}(\tau) = e^{\tau\hat{\mathcal{V}}}\hat{\mathcal{T}}e^{-\tau\hat{\mathcal{V}}}, \quad \hat{\mathcal{G}}(\tau) = e^{\tau\hat{\mathcal{V}}}\hat{\mathcal{G}}e^{-\tau\hat{\mathcal{V}}}. \tag{7}$$

The main advantage of sampling this extended partition function is the possibility to measure high-order correlation functions, such as n-points Green functions. In addition, the strength of the SGF algorithm is the possibility to simulate Hamilto-

nians with high-order terms that cannot be treated by other methods, e. g., many species systems with transmutation. Also, this algorithm works in any dimension in both the canonical and grand-canonical ensembles with an acceptance rate of the global updates of 100% for any Hamiltonian. All details about the SFG algorithm are discussed in Refs. (Rousseau, 2008).

We now discuss the application to the SGF algorithm for the study of Hamiltonian Eq. (1). The aim is to emphasize the capacity of this method to bring reliable results far from approximate methods, typically the mean-field approximation largely used in the literature. The mean-field phase diagram of Eq. (1) for many values of the quadratic Zeeman parameter q is plotted in Fig. 1 (a). We observe incompressible Mott insulator (MI) lobes with density $\rho = 1, 2$ (in black for $q/U_0 = 100$), and a compressible superfluid phase otherwise. The false colors show the total condensate fraction $C^{MF} = \sum_\sigma |\langle a_\sigma \rangle|^2$, i. e., the signature of a quantum liquid, for $q/U_0 = 100$. The interesting fact is that the boundary of the $\rho = 2$ MI lobe is tunable with q. Also, the nature of the quantum phase transition changes with q: dashed (plain) lines indicate first (second) order transitions. The mean-field phase diagram of Eq. (1) takes few minutes to be calculated, but is not reliable for low dimensional systems (the higher is the dimensionality, the higher is the mean-field accuracy).
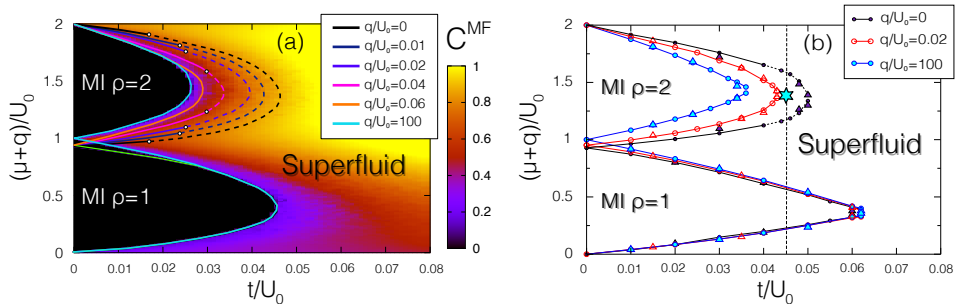

Figure 1: (Color online) (a) Mean field and (b) exact QMC phase diagram of model Eq. (1) for $L = 8$ (circles) and $L = 12$ (triangles) with respect to the quadratic Zeeman parameter q. Two phases are present: the Mott insulator (MI) with ρ particle per site and the superfluid phase. Contrary to the $\rho = 1$ MI region, q strongly affects the tip of the $\rho = 2$ Mott lobe. The dashed (plain) lines indicate a first- (second-) order transition. (a) False colors show the total condensate fraction $C^{MF} = \sum_\sigma |\langle a_\sigma \rangle|^2$ for $q/U_0 = 100$ and white dots indicate tricritical points. (b) The cyan star indicates the parameters chosen in Fig. 2.

The exact QMC phase diagram, using the SGF algorithm, is plotted in Fig. 1 (b). Such a plot takes less than 4 days to be calculated for many sizes L with parallelized simulations on the NEMO cluster. As expected, we observe MI and superfluid phases, and the shape of the diagrams is roughly the same as the mean-field ones (nevertheless, the QMC $\rho = 1$ MI lobe is sharper). The main difference is quantitative: the mean field is known for minimizing the quantum fluctuations. As a consequence, the tip of the MI lobe, where the MI-superfluid transition takes place, qualitatively differs: $t_c/U_0{}^{MF} < t_c/U_0{}^{QMC}$. The nature of the quantum phase transition also differs: the mean field suggests a first-order MI-superfluid transition at the tip of the Mott lobe for $\rho = 2$ and $q/U_0 = 0.02$. This statement is invalidated by our QMC results (Forges de Parny and Rousseau, 2018).
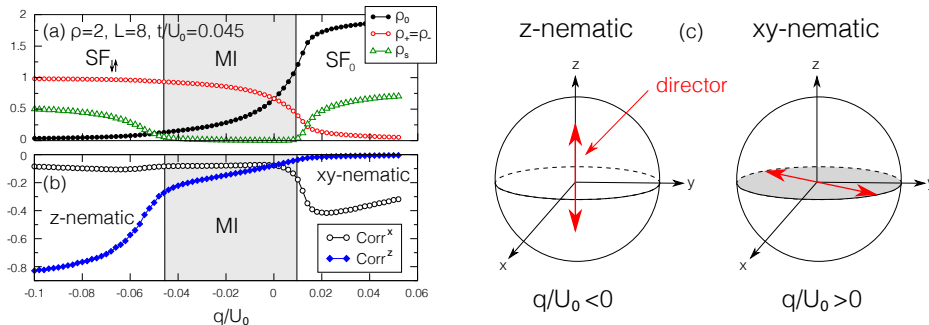

Figure 2: (Color online) (a) QMC data for $\rho = 2$ and $L = 8$ at fixed hopping $t/U_0 = 0.045$: q acts as a control parameter for the MI-SF transition. For $q \to -\infty$ the system is in the SF$_{\downarrow\uparrow}$ with a nematic director along z-axis and enters in the MI phase at $q/U_0 \simeq -0.045$ when increasing q. Then, the system continuously adopts a SF$_0$ phase with a nematic director belonging to the xy-plane at $q/U_0 \simeq 0.01$. Both transitions are second order. (b) Sketch of the two observed nematic structures.

The QMC method also allows us to prove that the quadratic Zeeman parameter is a control parameter for both the MI-superfluid transition and for the nematic structure. To emphasize this effect, we fix $t/U_0 = 0.045$ such that the system is in the MI phase for $q = 0$ (cyan star in Fig. 1 (b)). Fig. 2 (a) shows how the spin populations evolve when varying q/U_0: for $q/U_0 \to -\infty$ ($+\infty$) the system is populated by spins $\sigma = \pm 1$ ($\sigma = 0$) only. More interestingly, q acts as a control parameter for the MI-superfluid transition: for $q \to -\infty$ the system is in the SF$_{\downarrow\uparrow}$ phase with a nematic director along z-axis and enters in the MI phase at $q/U_0 \simeq -0.045$ when increasing q. Then, the system continuously adopts a SF$_0$ phase with a nematic

director belonging to the xy-plane at $q/U_0 \simeq 0.01$. Both transitions are second order. The superfluid phase is indicated by a non-zero superfluid density ρ_s. The structure of the nematic order is captured by the spin-spin correlation functions $\text{Corr}^\alpha = \frac{1}{L^4} \sum_{\mathbf{r}, R \neq 0} \langle \hat{S}_{\alpha, \mathbf{r}} \hat{S}_{\alpha, \mathbf{r}+R} \rangle \neq 0$, with $\alpha = x, y, z$, and $\text{Corr}^x = \text{Corr}^y$, plotted in Fig. 2 (b). The spins anti-align along a director oriented in the z axis for $q/U_0 < 0$ ($\text{Corr}^z \neq 0$), whereas the nematic director belongs to the xy plane for $q/U_0 > 0$ ($\text{Corr}^{x,y} \neq 0$). The two nematic structures observed are drawn in Fig. 2 (c). These spin-spin correlation functions are not accessible with the mean-field theory.

3 GMC method: application to ultracold gases with infinite-range cavity-mediated interactions

As in Sec. 2, we discuss an extended Bose-Hubbard model implemented in ultracold atoms experiments. We especially focus on a system recently investigated in the Esslinger's group at ETH-Zurich (Landig et al., 2016), where a cloud of cold atoms is placed in an optical lattice and inside a high-finesse optical cavity. The field of the cavity mediates an effective infinite-range interaction between the atoms, which favors a density difference between neighboring sites of the optical lattice. This experiment attracted a strong interest as it provides one of the first observations of the elusive *supersolid phase*, a phase initially discussed by Penrose and Onsager in 1956 (Penrose et al., 1956; Gross, 1957). The supersolid phase is characterized by both long-range phase coherence and spatial ordering, i.e., simultaneous diagonal and off-diagonal long-range orders. Our motivation was to bring additional and crucial information regarding the thermodynamic stability of the supersolid phase and elucidate the nature of the quantum phase transitions.

The experimental system is well described by the extended Bose-Hubbard model with an additional long-range interaction (Landig et al., 2016)

$$\hat{\mathcal{H}} = \underbrace{-t \sum_{\langle i,j \rangle} \left(a_i^\dagger a_j + \text{H.c.} \right)}_{\text{kinetic term}} + \underbrace{\frac{U_s}{2} \sum_{i \in e, o} \hat{n}_i \left(\hat{n}_i - 1 \right)}_{\text{on-site repulsion}}$$
$$\underbrace{- \frac{U_l}{K} \left(\sum_{i \in e} \hat{n}_i - \sum_{i \in o} \hat{n}_i \right)^2}_{\text{long-range interaction}} - \underbrace{\mu \sum_{i \in e, o} \hat{n}_i}_{\text{chemical potential}}. \tag{8}$$

This model describes spinless bosons on a square optical lattice inside a high-finesse optical cavity. The first term corresponds to the kinetic energy with tunneling amplitude t between nearest neighboring sites $\langle i, j \rangle$ defined on a square lattice with periodic boundary conditions and $L \times L$ sites. The kinetic term favors delocalization of bosons on the lattice and supports the superfluidity. The bosonic operator $a_i^\dagger$ (a_i) creates (annihilates) an atom at site i, and $\hat{n}_i = a_i^\dagger a_i$ is the corresponding number operator. The second term represents the on-site repulsive interactions between the atoms with strength $U_s > 0$. The index e and o denote respectively even and odd lattice sites. The third term describes the long-range interaction with amplitude $U_l > 0$ and favours imbalanced populations between even and odd sites, i. e. density oscillation. Finally, μ denotes the chemical potential.

The experimental phase diagram, plotted in Fig. 3, comprises four phases. For large negative detuning, the system adopts the superfluid phase for small interaction U_s/t, and the Mott insulator otherwise.
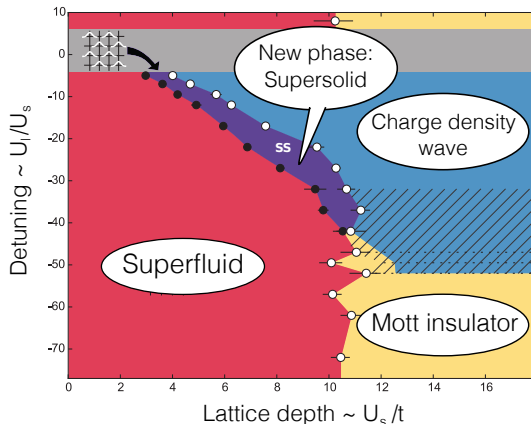

Figure 3: (Color online) Experimental phase diagram of Eq. (8) for one particle per site. Four phases are observed: a superfluid and a Mott insulator for small U_l, and a charge density wave and a supersolid phase for larger U_l. Taken from Ref. (Landig et al., 2016).

When the long-range interactions are turned on, the Mott insulator evolves in the charge density wave, i. e., an insulating phase with density oscillation, and more interestingly, a supersolid phase appears. The supersolid supports both the phase coherence of the superfluid and the density oscillation of the charge density wave. In

the experimental study, the stability of the supersolid remained an open question. Also, the nature of the quantum phase transitions has not been fully elucidated.

In this context, we have performed numerical simulations to tackle these questions. More generally, the understanding of the spectral properties of Hamiltonian Eq. (8) has been extensively studied in our group by Jonas Mielke (MSc Thesis, 2018). At the ground state level, we have used QMC simulations, with the SGF algorithm discussed in Sec. 2, and developed an improved mean-field method, the Gutzwiller Monte Carlo method (Flottat et al., 2017). The GMC and QMC phase diagrams are respectively plotted in Fig. 4 (a) and (b).
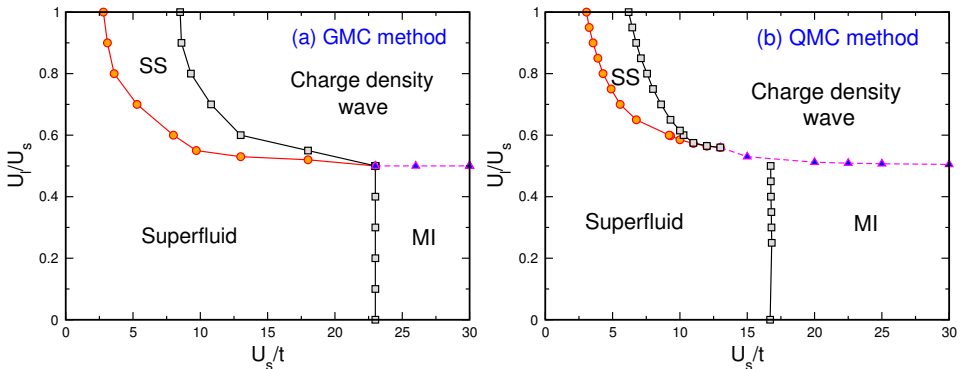

Figure 4: (Color online) (a) Zero temperature mean-field GMC and (b) exact QMC phase diagrams from Ref. (Flottat et al., 2017). The four experimental phases of Fig. 3 are found in both GMC and QMC phase diagrams. The QMC method reports a smaller SS region than the GMC one. Also, the superfluid to charge density wave transition is not observed in the GMC phase diagram.

As expected, we observe the four experimental phases of Fig. 3, namely the superfluid, the supersolid, the Mott insulator and the charge density wave. Both methods allow us to prove the stability of the supersolid phase with one particle per site and we unveiled the nature of the quantum phase transitions with QMC simulations. The differences observed in Fig. 4 (a) and (b) are not surprising since the GMC does not take into account the quantum fluctuations and therefore minimizes the critical hopping at the Mott-superfluid transition, i.e., $t_c^{GMC} < t_c^{QMC}$, then $U_s/t_c^{GMC} \sim 23 > U_s/t_c^{QMC} \sim 16$. This reason explains the size difference of the SS phase in Fig. 4 (a) and (b), i.e., the SS region is smaller in Fig. 4 (b). Also, the GMC methods does not allow for the direct observation of the superfluid to charge density wave transition. Nevertheless, the GMC method present real advantages:

- 3D systems are investigable (otherwise difficult with QMC);
- give access to the correlation functions (not standard in other mean-field formulations);
- gauge fields are investigable;
- take into account the thermal fluctuations in exact fashion;
- describes the Ising, XY and Berezinskii-Kosterlitz-Thouless transitions at finite temperature;
- easy to implement and requires small CPU and RAM resources (Fig. 4 (a) took less than 24h CPU).

We now describe the GMC method, based on Ref. (Hickey et al., 2014), developed by L. de Forges de Parny and T. Roscilde at ENS Lyon. This numerical method is built on the combination of both the Gutzwiller ansatz and the classical Monte Carlo method with Metropolis algorithm (Metropolis et al., 1953). This results in a *semi-classical lattice field theory* which preserves the U(1) symmetry, i.e. the gauge invariance, which is a great advantage compared to most of the mean-field approaches used in the literature. This method also allows for the *artificial reconstruction* of correlation functions on a $L \times L$ lattice cluster. More explicitly, the Gutzwiller mean-field state, written in the Fock basis $\{|\boldsymbol{n}_i\rangle\}$ with upper truncation n_{max}, takes the form

$$|\Psi(\mathbf{f})\rangle = \bigotimes_{i=1}^{L^2} |\psi_i\rangle = \bigotimes_{i=1}^{L^2} \left(\sum_{\boldsymbol{n}_i=0}^{n_{\max}} f_{\boldsymbol{n}_i}^{(i)} |\boldsymbol{n}_i\rangle \right) \ , \tag{9}$$

where L^2 is the total number of sites and $\mathbf{f} = \{f_{\boldsymbol{n}_i}^{(i)}\}$ is a vector of $(n_{\max} + 1) \times L^2$ complex coefficients, satisfying the normalization constraints $\sum_{\boldsymbol{n}} |f_{\boldsymbol{n}}^{(i)}|^2 = 1$ on each site. Because of this constraints, we have that

$$f_{\boldsymbol{n}_i}^{(i)} = A_{\boldsymbol{n}_i}^{(i)} e^{i\phi_{\boldsymbol{n}_i}^{(i)}} \tag{10}$$

with $0 \leq A_{\boldsymbol{n}_i}^{(i)} \leq 1$. In the program, the amplitudes $A_{\boldsymbol{n}_i}^{(i)}$ and phases $\phi_{\boldsymbol{n}_i}^{(i)}$ are long float numbers stored in two arrays of dimension $(n_{\max} + 1) \times L^2$, which is not a constraint for the sizes we have investigated ($L < 100$).

The GMC method consists of updating both the amplitudes $A_{\boldsymbol{n}_i}^{(i)}$ and the phases $\phi_{\boldsymbol{n}_i}^{(i)}$ using the metropolis algorithm with energy $E(\mathbf{f}) = \langle \Psi(\mathbf{f})|\hat{\mathcal{H}}|\Psi(\mathbf{f})\rangle$ which takes the explicit form

$$
\begin{aligned}
E(\mathbf{f}) \;=\; & -2t \sum_{\langle i,j\rangle} \sum_{\boldsymbol{n}_i,\boldsymbol{n}_j} \gamma_{ij}(\boldsymbol{n}_i,\boldsymbol{n}_j) \cos\left(\Delta\phi_{ij}(\boldsymbol{n}_i,\boldsymbol{n}_j)\right) \\
& + \sum_i \sum_{\boldsymbol{n}_i} (A_{\boldsymbol{n}_i}^{(i)})^2 \left[\frac{U_s}{2} n_i(n_i-1) - \mu n_i \right] \\
& - \frac{U_l}{K} \left(\sum_{i\in e}\sum_{\boldsymbol{n}_i} (A_{\boldsymbol{n}_i}^{(i)})^2 n_i - \sum_{i\in o}\sum_{\boldsymbol{n}_i} (A_{\boldsymbol{n}_i}^{(i)})^2 n_i \right)^2 ,
\end{aligned}
\tag{11}
$$

with

$$
\begin{aligned}
\gamma_{ij}(\boldsymbol{n}_i,\boldsymbol{n}_j) \;=\; & \sqrt{n_i n_j}\; A_{\boldsymbol{n}_i}^{(i)} A_{\boldsymbol{n}_i-1}^{(i)} A_{\boldsymbol{n}_j}^{(j)} A_{\boldsymbol{n}_j-1}^{(j)}, \\
\Delta\phi_{ij}(\boldsymbol{n}_i,\boldsymbol{n}_j) \;=\; & \left(\phi_{\boldsymbol{n}_i}^{(i)} - \phi_{\boldsymbol{n}_i-1}^{(i)} \right) - \left(\phi_{\boldsymbol{n}_j}^{(j)} - \phi_{\boldsymbol{n}_j-1}^{(j)} \right) .
\end{aligned}
\tag{12}
$$

The above model, Eq. (12), represents the Hamiltonian of a generalized XY model with fluctuating couplings. The XY spins live on a $(2D+1)$-dimensional lattice with sites $(i, \boldsymbol{n}_i)$, where the extra dimension is provided by the occupation number. At the heart of Gutzwiller Monte Carlo is the simplification of the Boltzmann weight:

$$
\langle \Psi(\mathbf{f})|\; e^{-\beta\hat{\mathcal{H}}}\; |\Psi(\mathbf{f})\rangle \to e^{-\beta E(\mathbf{f})}.
\tag{13}
$$

The classical Monte Carlo simulation contains two kinds of single-site Metropolis moves: amplitude moves, preserving the sum constraint, and phase moves. A subtle aspect concerns the transition probabilities for amplitude moves as the amplitude appears in the metric of the integrals defining the partition function with a linear term of the kind $A_{\boldsymbol{n}_i}^{(i)} = \exp[\log(A_{\boldsymbol{n}_i}^{(i)})]$. This means that an amplitude move on site i, changing $\{A_{\boldsymbol{n}_i}^{(i)}\}$ into $\{A_{\boldsymbol{n}_i}'^{(i)}\}$, has to be accepted with probability

$$
P = \min\left(e^{-\beta[E(\{A_{\boldsymbol{n}_i}'^{(i)}\}) - E(\{A_{\boldsymbol{n}_i}^{(i)}\})]} \times e^{\sum_{\boldsymbol{n}_i} \ln(A_{\boldsymbol{n}_i}'^{(i)}/A_{\boldsymbol{n}_i}^{(i)})}, 1 \right).
\tag{14}
$$

Our simulations were performed on a square lattice of size $L \times L$ with periodic boundary conditions. The average total energy is given by $E = \langle E(\mathbf{f})\rangle$ and the total density is defined by $\rho = \frac{1}{L^2}\langle \sum_i \sum_{\boldsymbol{n}_i} n_i (A_{\boldsymbol{n}_i}^{(i)})^2 \rangle$, where $\langle . \rangle \equiv \frac{1}{N_{\mathrm{MC}}} \sum_n^{N_{MC}} (.)$

is the Monte Carlo average. This part is implemented by a loop in the program. The signature of a long-range order phase coherence is given by a finite condensate fraction $C = \frac{1}{L^4} \sum_{i,j} \langle a_i^\dagger a_j \rangle$ given by

$$
\begin{aligned}
C = \quad & \frac{1}{L^4} \left\langle \left[\sum_{i,\boldsymbol{n}_i} \gamma_i(\boldsymbol{n}_i) \cos(\phi_{\boldsymbol{n}_i}^{(i)} - \phi_{\boldsymbol{n}_i-1}^{(i)}) \right]^2 \right\rangle \\
& + \frac{1}{L^4} \left\langle \left[\sum_{i,\boldsymbol{n}_i} \gamma_i(\boldsymbol{n}_i) \sin(\phi_{\boldsymbol{n}_i}^{(i)} - \phi_{\boldsymbol{n}_i-1}^{(i)}) \right]^2 \right\rangle ,
\end{aligned}
\tag{15}
$$

with $\gamma_i(\boldsymbol{n}_i) = \sqrt{n_i} \, A_{\boldsymbol{n}_i}^{(i)} A_{\boldsymbol{n}_i-1}^{(i)}$. The phase coherence signal is also captured by the superfluid density ρ_s, defined as the second derivative of the free-energy density $f = -\frac{1}{L^2 \beta} \log \mathcal{Z}$ with respect to a phase twist φ of the creation and annihilation operators along a given (x) direction such that $a_x^\dagger \to a_x^\dagger e^{i\varphi x/L}$ and $a_x \to a_x e^{-i\varphi x/L}$, and with $\mathcal{Z}$ the partition function and $\beta = 1/k_B T$. The superfluid density reads

$$
\rho_s = \left. \frac{\partial^2 f}{\partial \varphi^2} \right|_{\varphi=0} = \frac{1}{L^2} \left\langle \frac{\partial^2 \mathcal{H}(\varphi)}{\partial \varphi^2} \right\rangle \bigg|_{\varphi=0} - \frac{\beta}{L^2} \left\langle \left(\frac{\partial \mathcal{H}(\varphi)}{\partial \varphi} \right)^2 \right\rangle \bigg|_{\varphi=0} .
\tag{16}
$$

In the framework of the GMC formulation and using the energy formulation Eq. (12), the superfluid density becomes

$$
\begin{aligned}
\rho_s = \quad & \frac{2t}{L^2} \left\langle \sum_{\langle i,j \rangle_x} \sum_{\boldsymbol{n}_i, \boldsymbol{n}_j} \gamma_{ij}(\boldsymbol{n}_i, \boldsymbol{n}_j) \cos(\Delta\phi_{ij}(\boldsymbol{n}_i, \boldsymbol{n}_j)) \right\rangle \\
& - \frac{4t^2}{TL^2} \left\langle \left(\sum_{\langle i,j \rangle_x} \sum_{\boldsymbol{n}_i, \boldsymbol{n}_j} \gamma_{ij}(\boldsymbol{n}_i, \boldsymbol{n}_j) \sin(\Delta\phi_{ij}(\boldsymbol{n}_i, \boldsymbol{n}_j)) \right)^2 \right\rangle ,
\end{aligned}
\tag{17}
$$

where $\gamma_{ij}(\boldsymbol{n}_i, \boldsymbol{n}_j)$ and $\Delta\phi_{ij}(\boldsymbol{n}_i, \boldsymbol{n}_j)$ are defined by Eqs. (12). The information of the spatial order is given by the structure factor $S(\mathbf{k})$, i.e. the Fourier transform of the density-density correlation function, $S(\mathbf{k}) = \frac{1}{L^2} \sum_{\mathbf{r},r'} e^{i\mathbf{k}.(r-r'))} \langle n_\mathbf{r} n_{\mathbf{r}'} \rangle$. Particularly, the density oscillations observed in the charge density wave and in the supersolid phases are signaled by $S(\pi, \pi) \neq 0$.

At finite temperature, we have obtained promising results. For instance, Fig. 5 shows the expected scaling behavior of the condensate fraction Eq. (15) at a Berezin-

skii-Kosterlitz-Thouless transition, i.e., $C(T_{BKT}) \propto L^{-1/4}$. Also, we observe the associated well-known universal jump of the superfluid density $\rho_s(T_{BKT}) = 2T_{BKT}/\pi$.
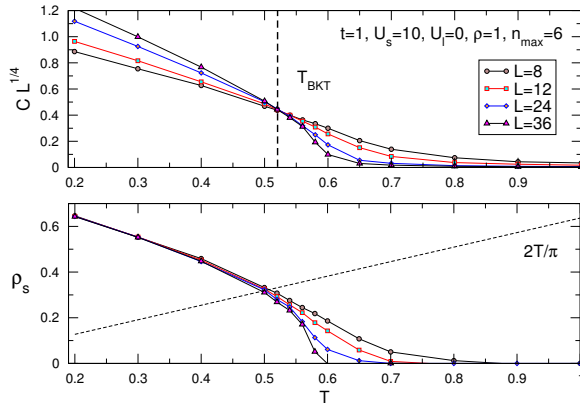

Figure 5: (Color online) (Up) Finite size scaling of the condensate fraction C, Eq. (15), and (down) of the superfluid density ρ_s, Eq. (17), as a function of the temperature T for the 2D standard Bose-Hubbard model ($U_l = 0$).

4 MCTDHX method: many-body tunneling dynamics of interacting bosons in a double well

This section reports on our numerical activities concerning quantum many-body dynamics of interacting bosons trapped in a double-well potential. This model has been extensively studied both experimentally and theoretically in the context of the Josephson oscillations in quantum gases experiments (Albiez et al., 2005). We have particularly focused on dynamical scenarios where the trap evolves in time from a single well to a double well by raising a central gaussian barrier with a ramping time T_{ramp}.

This system is modeled by N interacting spinless bosons of mass m trapped in a one-dimensional double well for which the many-body Hamiltonian reads

$$\hat{\mathcal{H}} \;=\; \sum_i^N \left(-\frac{1}{2}\frac{d^2}{dx_i^2} + V(x_i,t) \right) + \frac{\lambda}{2}\sum_{i\neq j} \delta(x_i - x_j) \; , \qquad (18)$$

with units $m = \hbar = 1$, and where the double-well potential

$$V(x_i, t) = \frac{x_i^2}{2} + A(t)e^{-x_i^2/2} \tag{19}$$

results from the combination of both a harmonic potential superimposed by a central gaussian barrier with time dependent amplitude $A(t)$ of the form

$$A(t) = A_{\max} \times \begin{cases} t/T_{\mathrm{ramp}}, & t < T_{\mathrm{ramp}}, \\ 1, & t \geq T_{\mathrm{ramp}}. \end{cases} \tag{20}$$

In Eq. (19), x_i denotes the coordinate of the ith particle. The repulsive inter-particle interaction strength, $\lambda > 0$, is determined by the s-wave scattering length a_s and the transverse confinement $\omega_\perp$ (Olshanii, 1998). The spectral structures and many-body tunneling dynamics of Hamiltonian Eq. (18) have been extensively studied in our group by Frank Schäfer in collaboration with Miguel Bastarrachea-Magnani (MSc Thesis, 2018). To this end, we have used many numerical methods. In this paper, we restrict our attention to the Multiconfigurational Time-dependent Hartree method for bosons (MCTDHX).

MCTDHX allows for the investigation of interacting particles in many scenarios, e. g. interacting bosons or fermions in optical lattices (Lode and Bruder, 2016) or bosons in double-well potentials (Zöllner et al., 2008; Zöllner et al., 2006; Streltsov et al., 2007). In our context, this method is useful for the investigation of N interacting bosons in a time-dependent double-well potential. Nevertheless, this method is not efficient for the calculation of the entire energy spectrum. In the following, we outline the basic steps towards the MCTDHX equations of motion, see Ref. (Alon et al., 2008) for extensive details regarding the method. The aim is to solve the time-dependent Schrödinger equation

$$i\frac{\partial}{\partial t}|\Psi\rangle = \hat{\mathcal{H}}|\Psi\rangle \ , \tag{21}$$

with many-body Hamiltonian $\hat{\mathcal{H}}$ defined by Eq. (18). To do so, we first formulate a general multiconfigurational ansatz for the wave function based on truncating the field operator

$$\Psi(x,t) = \sum_{k=1}^{\infty} a_k(t)\phi_k(x,t) \tag{22}$$

from an infinite to a finite sum of M operators, i.e.,

$$\Psi(x,t) = \sum_{k=1}^{M} a_k(t)\phi_k(x,t) \ . \tag{23}$$

Under this assumption, the bosonic ansatz for the many-body wave function reads

$$|\Psi\rangle = \sum_{\{\vec{n}\}} C_{\vec{n}}(t) \prod_{k=1}^{M} \frac{(a_k^{\dagger}(t))^{n_k}}{\sqrt{n_k!}} |vac.\rangle, \tag{24}$$

where the summation runs over all (symmetrized) basis states of the Hilbert space. The vector $\vec{n} = (n_1, n_2, \ldots, n_M)$ represents the occupations of the orbitals that preserve the total number of particles $n_1 + n_2 + n_3 + \cdots + n_M = N$, M is the number of orbitals $\phi_k(x,t)$, and $|vac.\rangle$ is the vacuum. The key idea of MCTDHX is to control the later assumption a posteriori to get a considerably reduction of the computational effort.

Using this ansatz, the time-dependent Schrödinger equation is solved by using the time-dependent variational principle for minimizing the action functional (Kramer et al., 1981)

$$\mathcal{S} = \int dt \left[\langle \Psi(t)| \left(\hat{\mathcal{H}} - i\frac{\partial}{\partial t} \right) |\Psi(t)\rangle - \sum_{k,j=1}^{M} \mu_{kj}(t) \Big(\langle \phi_k(t)|\phi_j(t)\rangle - \delta_{kj} \Big) \right], \tag{25}$$

where the time-dependent Lagrange multipliers $\mu_{kj}(t)$ enforce the orthonormality of the orbitals. The minimization of the action $\mathcal{S}$ finally leads to the MCTDHX

equations of motion, i. e., a coupled set of first-order non-linear differential equations (Alon et al., 2008)

$$
\begin{aligned}
i\frac{\partial}{\partial t}C_{\vec{n}}(t) &= \sum_{\vec{m}} \langle \vec{n},t| \left(\hat{\mathcal{H}} - i\frac{\partial}{\partial t} \right) |\vec{m},t\rangle C_{\vec{m}}(t) \\
i\frac{\partial}{\partial t}|\phi_k\rangle &= \mathbf{P} \bigg[\left(-\frac{1}{2}\frac{d^2}{dx^2} + V(x,t) \right)|\phi_k\rangle \\
&\quad + \lambda \sum_{\alpha\beta\gamma\delta}^{M} \{\rho^{(1)}\}_{k\alpha}^{-1}\rho_{\alpha\beta\gamma\delta}^{(2)}\phi_\beta^*(x,t)\phi_\delta(x,t)|\phi_\gamma\rangle \bigg],
\end{aligned}
\tag{26}
$$

where $\mathbf{P} = 1 - \sum_{j=1}^{M}|\phi_j\rangle\langle\phi_j|$ denotes the projection operator, and where $\rho_{k\alpha}^{(1)} = \langle\Psi|a_k^\dagger a_\alpha|\Psi\rangle$ and $\rho_{\alpha\beta\gamma\delta}^{(2)} = \langle\Psi|a_\alpha^\dagger a_\beta^\dagger a_\gamma a_\delta|\Psi\rangle$ are respectively the matrix elements of the reduced single- and two-particle density matrices. The projector $\mathbf{P}$ vanishes *exactly* only in the limit $M \to \infty$, thus Eq. (26) becomes equivalent to the time-dependent Schrödinger equation. On the other side, the MCTDHX method with one orbital, i. e., $M = 1$, is equivalent to the Gross-Pitaevskii mean field where only one coefficient $C_{0,0,..,N,..,0}(t)$ contributes. Therefore, the accuracy of MCTDHX strongly depends on the choice of the number of orbitals M used in the simulations and the convergence of the MCTDHX results can be improved by increasing the number of orbitals M (Lode and Bruder, 2016).

We have used the freely available software implementation (Lode, Tsatsos et al., 2017), where the spatial discretization relies on a discrete variable representation (DVR) combined with a fast Fourier transformation (Beck et al., 2000). In practice, we have used $M = 20$ orbitals, $x_{max} = -x_{min} = 12$ and $NDVR_x = 512$ grid points. With this choice of parameters, the convergence of the MCTDHX results for two interacting bosons in a harmonic trap, with respect to the exact ones, is found of the order of 10^{-4}–10^{-2}. See Refs. (Lode and Bruder, 2016; Lode, Sakmann et al., 2012; Fasshauer et al., 2016) for more details on the convergence of the method.

As an example, MCTDHX allows for the observation of different dynamical scenarios as a function of the ramping time T_{ramp}. We observe saturation or oscillations of the von Neumann entropy

$$
S(t) = -\text{Tr}\left[\rho^{(1)}(t)\ln\rho^{(1)}(t)\right] ,
\tag{27}
$$

with $\rho^{(1)}(t)$ the reduced single-particle density matrix. As shown in Fig. 6, this statement is observed from $N = 2$ to $N = 100$ particles.
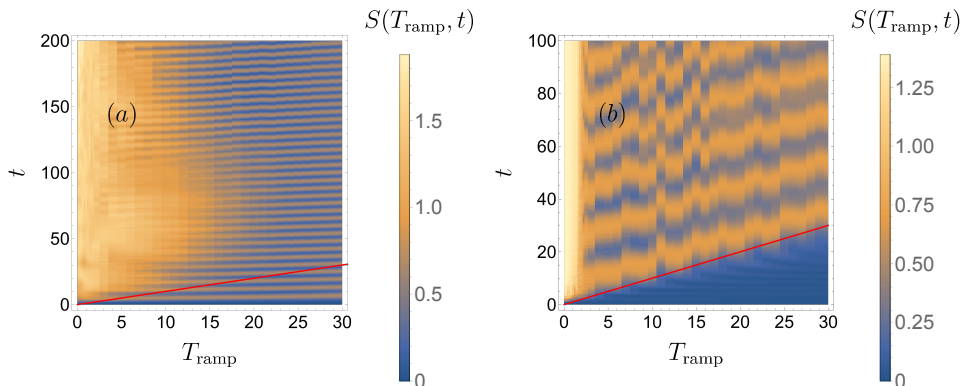

Figure 6: (Color online) Time evolution of the von Neumann entropy in false colors as a function of the ramping time T_{ramp} in the case of (a) 2 particles and (b) 100 particles with interaction $\lambda = 1$. Above the red line, $t = T_{ramp}$, the double-well potential is fixed.

In the saturating regime, the larger the interaction strength, the faster the entropy converges to the equilibrium value. In the oscillating regime, the oscillation has a well-defined frequency determined by the energy gap of the ground state with respect to the first excited state as $\nu(\lambda) = (E_1 - E_0)/\pi$.

5 Conclusion

We have presented a panel of the numerical methods employed in the Quantum Optics and Statistics department at the University of Freiburg's Institute of Physics between September 2016 and June 2018. Particularly, we have discussed three fundamentally different methods in three physical contexts:

(1) We have presented the quantum Monte Carlo method with the stochastic Green function algorithm. The advantages of using this method compared to the mean-field one in the context of quantum magnetism have been discussed. This exact method allowed us to derive the phase diagram of a spin-1 Bose-Hubbard model (Forges de Parny and Rousseau, 2018).

(2) We have described a new method we have developed: the Gutzwiller Monte Carlo (Flottat et al., 2017). This flexible variational method consists of a lattice field theory associated with a Metropolis Monte Carlo method. This method reduces to an extended mean field at zero temperature, but takes into account the thermal fluctuations at finite temperature. We highlighted the use of this method in the context of ultracold gases with infinite-range cavity-mediated interactions, a system under investigation in our group, see J. Mielke's MSc thesis, 2018.

(3) Lastly, we have presented the Multiconfigurational Time-dependent Hartree method for bosons in the context of many-body dynamics of interacting bosons in a double well, see F. Schäfer's MSc thesis, 2018. This method is particularly suited for the investigation of the dynamics of interacting bosons and fermions in many physical contexts.

Each method has its own strengths and limitations which have to be considered depending on the system under investigation. In quantum mechanics, the main constraint remains the diagonalization of the (huge) Hamiltonian matrix, a mathematical operation circumvented by the technics described in this paper. Nowadays, many perspectives are considered: algorithms based on machine learning, tensor networks and the time-DMRG – already used but still restricted at short time – and a direct quantum treatment with quantum computers, e. g., D-wave.

Acknowledgement

Corresponding Author

Andreas Buchleitner: `abu@uni-freiburg.de`

Physikalisches Institut, Albert-Ludwigs-Universität Freiburg,

Hermann-Herder-Straße 3, 79104 Freiburg, Germany

References

Albiez, M. et al. (2005). »Direct Observation of Tunneling and Nonlinear Self-Trapping in a Single Bosonic Josephson Junction«. In: *Phys. Rev. Lett.* 95 (1), p. 010402. DOI: `10.1103/PhysRevLett.95.010402`.

Alon, O. E., A. I. Streltsov and L. S. Cederbaum (2008). »Multiconfigurational time-dependent Hartree method for bosons: Many-body dynamics of bosonic systems«. In: *Phys. Rev. A* 77 (3), p. 033613. DOI: `10.1103/PhysRevA.77.033613`.

Beck, M. H., A. Jäckle, G. A. Worth and H.-D. Meyer (2000). »The multiconfiguration time-dependent Hartree (MCTDH) method: a highly efficient algorithm for propagating wavepackets«. In: *Physics Reports* 324.1, pp. 1–105. ISSN: 0370-1573. DOI: `10.1016/S0370-1573(99)00047-2`.

Bloch, I., J. Dalibard and W. Zwerger (2008). »Many-body physics with ultracold gases«. In: *Rev. Mod. Phys.* 80 (3), pp. 885–964. DOI: `10.1103/RevModPhys.80.885`.

Dagotto, E. (1994). »Correlated electrons in high-temperature superconductors«. In: *Rev. Mod. Phys.* 66 (3), pp. 763–840. DOI: `10.1103/RevModPhys.66.763`.

Dauxois, T., M. Peyrard and S. Ruffo (2005). »The Fermi–Pasta–Ulam 'numerical experiment': history and pedagogical perspectives«. In: *European Journal of Physics* 26.5, S3. URL: `http://stacks.iop.org/0143-0807/26/i=5/a=S01`.

Fasshauer, E. and A. U. J. Lode (2016). »Multiconfigurational time-dependent Hartree method for fermions: Implementation, exactness, and few-fermion tunneling to open space«. In: *Phys. Rev. A* 93 (3), p. 033635. DOI: `10.1103/PhysRevA.93.033635`.

Fehske, H., R. Schneider and A. Weiße (2007). *Computational Many-Particle Physics, Lecture Notes in Physics*. Ed. by Springer. Springer, Berlin, Heidelberg.

Ferrario, M., G. Ciccotti and K. Binder (2006). *Computer Simulations in Condensed Matter Systems: From Materials to Chemical Biology Volume 1*. Ed. by Springer. Springer, Berlin, Heidelberg.

Fisher, M. P. A., P. B. Weichman, G. Grinstein and D. S. Fisher (1989). »Boson localization and the superfluid-insulator transition«. In: *Phys. Rev. B* 40 (1), pp. 546–570. DOI: `10.1103/PhysRevB.40.546`.

Flottat, T., L. de Forges de Parny, F. Hébert, V. G. Rousseau and G. G. Batrouni (2017). »Phase diagram of bosons in a two-dimensional optical lattice with infinite-range cavity-mediated interactions«. In: *Phys. Rev. B* 95 (14), p. 144501. DOI: `10.1103/PhysRevB.95.144501`.

Forges de Parny, L. de, F. Hébert, V. G. Rousseau and G. G. Batrouni (2013). »Interacting spin-1 bosons in a two-dimensional optical lattice«. In: *Phys. Rev. B* 88 (10), p. 104509. DOI: `10.1103/PhysRevB.88.104509`.

Forges de Parny, L. de and V. G. Rousseau (2018). »Phase diagrams of antiferromagnetic spin-1 bosons on a square optical lattice with the quadratic Zeeman effect«. In: *Phys. Rev. A* 97 (2), p. 023628. DOI: `10.1103/PhysRevA.97.023628`.

Forges de Parny, L. de, H.-Y. Yang and F. Mila (2014). »Anderson Tower of States and Nematic Order of Spin-1 Bosonic Atoms on a 2D Lattice«. In: *Phys. Rev. Lett.* 113 (20), p. 200402. DOI: `10.1103/PhysRevLett.113.200402`.

Greiner, M., O. Mandel, T. Esslinger, T. W. Hänsch and I. Bloch (2002). »Quantum phase transition from a superfluid to a Mott insulator in a gas of ultracold atoms«. In: *Nature* 415 (15), pp. 39–44. DOI: `10.1038/415039a`.

Gross, E. P. (1957). »Unified Theory of Interacting Bosons«. In: *Phys. Rev.* 106 (1), pp. 161–162. DOI: `10.1103/PhysRev.106.161`.

Hickey, C. and A. Paramekanti (2014). »Thermal Phase Transitions of Strongly Correlated Bosons with Spin-Orbit Coupling«. In: *Phys. Rev. Lett.* 113 (26), p. 265302. DOI: `10.1103/PhysRevLett.113.265302`.

Ho, T.-L. (1998). »Spinor Bose Condensates in Optical Traps«. In: *Phys. Rev. Lett.* 81 (4), pp. 742–745. DOI: `10.1103/PhysRevLett.81.742`.

Imambekov, A., M. Lukin and E. Demler (2003). »Spin-exchange interactions of spin-one bosons in optical lattices: Singlet, nematic, and dimerized phases«. In: *Phys. Rev. A* 68 (6), p. 063602. DOI: `10.1103/PhysRevA.68.063602`.

— (2004). »Magnetization Plateaus for Spin-One Bosons in Optical Lattices: Stern-Gerlach Experiments with Strongly Correlated Atoms«. In: *Phys. Rev. Lett.* 93 (12), p. 120405. DOI: `10.1103/PhysRevLett.93.120405`.

Jacob, D. et al. (2012). »Phase diagram of spin-1 antiferromagnetic Bose-Einstein condensates«. In: *Phys. Rev. A* 86 (6), p. 061601. DOI: `10.1103/PhysRevA.86.061601`.

Jaksch, D., C. Bruder, J. I. Cirac, C. W. Gardiner and P. Zoller (1998). »Cold Bosonic Atoms in Optical Lattices«. In: *Phys. Rev. Lett.* 81 (15), pp. 3108–3111. DOI: `10.1103/PhysRevLett.81.3108`.

Jiang, J. et al. (2016). »First-order superfluid-to-Mott-insulator phase transitions in spinor condensates«. In: *Phys. Rev. A* 93 (6), p. 063607. DOI: `10.1103/PhysRevA.93.063607`.

Kramer, P. and M. Saraceno (1981). »Geometry of the Time-Dependent Variational Principle in Quantum Mechanics«. In: *Lecture Notes in Physics* 140.

Landig, E. et al. (2016). »Quantum phase transition from a superfluid to a Mott insulator in a gas of ultracold atoms«. In: *Nature* 532, pp. 476–479. DOI: `10.1038/nature17409`.

Lode, A. U. J. and C. Bruder (2016). »Dynamics of Hubbard Hamiltonians with the multiconfigurational time-dependent Hartree method for indistinguishable particles«. In: *Phys. Rev. A* 94 (1), p. 013616. DOI: `10.1103/PhysRevA.94.013616`.

Lode, A. U. J., K. Sakmann, O. E. Alon, L. S. Cederbaum and A. I. Streltsov (2012). »Numerically exact quantum dynamics of bosons with time-dependent interactions of harmonic type«. In: *Phys. Rev. A* 86 (6), p. 063606. DOI: `10.1103/PhysRevA.86.063606`.

Lode, A. U. J., M. C. Tsatsos and E. Fasshauer (2017). *MCTDH-X: The time-dependent multiconfigurational Hartree for indistinguishable particles software.* URL: `http://ultracold.org`.

Loh, E. Y. et al. (1990). »Sign problem in the numerical simulation of many-electron systems«. In: *Phys. Rev. B* 41 (13), pp. 9301–9307. DOI: `10.1103/PhysRevB.41.9301`.

Mahmud, K. W. and E. Tiesinga (2013). »Dynamics of spin-1 bosons in an optical lattice: Spin mixing, quantum-phase-revival spectroscopy, and effective three-body interactions«. In: *Phys. Rev. A* 88 (2), p. 023602. DOI: `10.1103/PhysRevA.88.023602`.

Metropolis, N., A. W. Rosenbluth, M. N. Rosenbluth, A. H. Teller and E. Teller (1953). »Equation of State Calculations by Fast Computing Machines«. In: *The Journal of Chemical Physics* 21.6, pp. 1087–1092. DOI: `10.1063/1.1699114`.

Nature Physics (2013). »The Hubbard model at half a century«. In: *Nature Physics* 9, p. 523. DOI: `10.1038/nphys2759`.

Olshanii, M. (1998). »Atomic Scattering in the Presence of an External Confinement and a Gas of Impenetrable Bosons«. In: *Phys. Rev. Lett.* 81 (5), pp. 938–941. DOI: `10.1103/PhysRevLett.81.938`.

Penrose, O. and L. Onsager (1956). »Bose-Einstein Condensation and Liquid Helium«. In: *Phys. Rev.* 104 (3), pp. 576–584. DOI: `10.1103/PhysRev.104.576`.

Román, O. (2014). »A practical introduction to tensor networks: Matrix product states and projected entangled pair states«. In: *Annals of Physics* 349, pp. 117–158. ISSN: 0003-4916. DOI: `10.1016/j.aop.2014.06.013`.

Rousseau, V. G. (2008). »Directed update for the stochastic Green function algorithm«. In: *Phys. Rev. E* 78 (5), p. 056707. DOI: `10.1103/PhysRevE.78.056707`.

Sandvik, A. W. (2010). »Computational Studies of Quantum Spin Systems«. In: *AIP Conf. Proc.* 1297, p. 135.

Scalapino, D. J. (2006). »Numerical Studies of the 2D Hubbard Model«. In: *Handbook of High Temperature Superconductivity*. arXiv: `cond-mat/0610710 [cond-mat.str-el]`.

Streltsov, A. I., O. E. Alon and L. S. Cederbaum (2007). »Role of Excited States in the Splitting of a Trapped Interacting Bose-Einstein Condensate by a Time-Dependent Barrier«. In: *Phys. Rev. Lett.* 99 (3), p. 030402. DOI: `10.1103/PhysRevLett.99.030402`.

Vengalattore, M., J. Guzman, S. R. Leslie, F. Serwane and D. M. Stamper-Kurn (2010). »Periodic spin textures in a degenerate $F = 1$ ^{87}Rb spinor Bose gas«. In: *Phys. Rev. A* 81 (5), p. 053612. DOI: `10.1103/PhysRevA.81.053612`.

Vengalattore, M., S. R. Leslie, J. Guzman and D. M. Stamper-Kurn (2008). »Spontaneously Modulated Spin Textures in a Dipolar Spinor Bose-Einstein Condensate«. In: *Phys. Rev. Lett.* 100 (17), p. 170403. DOI: `10.1103/PhysRevLett.100.170403`.

Zibold, T. et al. (2016). »Spin-nematic order in antiferromagnetic spinor condensates«. In: *Phys. Rev. A* 93 (2), p. 023614. DOI: `10.1103/PhysRevA.93.023614`.

Zöllner, S., H.-D. Meyer and P. Schmelcher (2006). »Ultracold few-boson systems in a double-well trap«. In: *Phys. Rev. A* 74 (5), p. 053612. DOI: `10.1103/PhysRevA.74.053612`.

— (2008). »Few-Boson Dynamics in Double Wells: From Single-Atom to Correlated Pair Tunneling«. In: *Phys. Rev. Lett.* 100 (4), p. 040401. DOI: `10.1103/PhysRevLett.100.040401`.